Supporting Information for the manuscript

Rational design of noble-metal-free cocatalysts for balanced H_2 adsorption-desorption and accelerated charge separation toward efficient light-driven hydrogen production

Jin-Ge Hao [a], Jun Wang [a], Kai Yang [a], Wei-Wei Zhu [a], Tao Deng [a], Kang-Qiang Lu [a*] and Yi-Jun Xu[b]

[a] Jiangxi Provincial Key Laboratory of Functional Crystalline Materials Chemistry, School of Chemistry and Chemical Engineering, Jiangxi University of Science and Technology, Ganzhou 341000, Jiangxi, China

[b] Institute of Fundamental and Frontier Sciences, University of Electronic Science and Technology of China, Chengdu 611731, China

*Corresponding authors: E-mail: kqlu@jxust.edu.cn

Experimental section

1.1 Preparation of pure GO

Synthesis of graphene oxide: GO was synthesized by a modified Hummers' method. In detail, 10 g graphite powder (supplied from Qingdao Zhong tian Company, China) was put into 230 mL concentrated H_2SO_4 under moderate stirring. Then, 30 g $KMnO_4$ was added gradually under stirring and the solution was cold below 5 °C in an ice bath. After that, the solution was heated to 35 °C in a water-bath and kept stirring for 2 h. Then, the mixture was diluted with 500 mL DI water in an ice bath to keep the temperature below 5 °C. Shortly after the further diluted with 1.5 L of DI water, 80 mL 30% H_2O_2 was then added into the mixture. The mixture was centrifuged and washed with 1:10 HCl aqueous solution to remove metal ions followed by DI water to remove the acid. After that, the mixture was dialyzed for one week and the final GO sample was obtained after full sonication.

1.2 Preparation of $Ni(OH)_2$-GR

Synthesis of Nickel hydroxide nanosheet arrays-graphene ($Ni(OH)_2$-GR) composites: firstly, a certain amount of GO was dispersed into 50 mL DI water with ultrasonication for 1h. Then, 2.5 mmol ($Ni(NO_3)_2 \cdot 6H_2O$) was dissolved into the GO solution and stirred for 0.5 h. Afterward, a 50 mL solution containing 0.25 mmol of $C_6H_5O_7Na_3$ and 2.5 mmol of HMTA was incorporated to the above-mixed solution and stirred for 1h. After that, the obtained solution was heated to 363 K and maintained for 10 h with vigorous agitation. Subsequently, when the solution temperature was cooled to 298 K, the sample was collected by centrifugation and washed thoroughly with DI water. After finally treated by freeze-drying, $Ni(OH)_2$-GR composites with different contents of GR (1, 5, 10, and 30 wt%) were obtained. In addition, bare GR was prepared using the same method in the absence of transition metal nitrate.

1.3 Characterizations

The structures of the samples were determined by dual beam SEM (Zeiss Sigma 500 instrument) and TEM (Jeol JEM-2100F instrument). XRD patterns were collected on a Rigaku Miniflex diffractometer with Cu Kα radiation. In addition, N_2 adsorption–desorption curves and distribution pore sizes were studied by using N_2 as the carrier gas in liquid nitrogen in an adsorption analyzer on a Micromeritics ASAP 2020. XPS tests were executed on Thermo Scientific Escalab 250 Xi spectrometer. Raman spectra were tested on a Renishaw in Via Raman System 1000 with a 532 nm Nd:YAG excitation source. Steady-state PL spectra of these samples were tested on Hitachi F-4500

fluorescence spectrometer. The above PL measurements were performed in H_2O/TEOA (5:1, 6mL) mixed solution containing 15 mg EY and 1 mg as-prepared cocatalysts. The excitation wavelength was 490 nm when steady-state PL was measured. Furthermore, all the cyclic voltammetry (CV) and linear sweep voltammetry (LSV) curves were carried out in the three-electrode cell, in which Ag/AgCl was used as reference electrode, a Pt wire was used as a counter electrode and an indiumtin oxide (ITO) conductive glass was used with the samples as a working electrode in 0.1 M Na_2SO_4 electrolyte (pH=6.8), all measurements were carried out on CH Instruments CHI-660E electrochemical workstation. EIS measurements were implemented on electrochemical workstation (CH Instruments CHI-660E). Contact angle measurements were carried out using the static drop method using a Fangrui Instrument Company JCY contact angle meter. Likewise, gas-solid phosphating was performed on the samples using a tube furnace (OTF-1200X).

1.4 Computational details for DFT calculations.

All DFT calculations were carried out by the Vienna ab initio Simulation Package (VASP).The Perdew-Burke-Ernzerhof (PBE) exchange-correlation functional and projector augmented wave (PAW) pseudopotential were adopted with spin-polarization. During the structure optimization, the convergence criterion of total energy was set to 10^{-6} eV, and the atoms were relaxed until the force acting on each atom was less than 0.01 eV/Å. Gaussian smearing of 0.05 eV to the orbital occupation is applied. A plane-wave cut-off energy of 500 eV was used in all computations. Brillouin-zone sampling was sampled with 3×3×1 Monkhorst-Pack grids. Each slab model was separated from its neighbors by 15 Å vacuum layer spacing. DFT-D3 method of Grimme with zero-damping function were used in van der Waals (vdW) corretions. The free energy profiles, which are efficient in estimating the performance of electrocatalytic reactions, were acquired by applying the computational electrode model (CHE).

The Gibbs free energies of the OER were calculated by correcting the DFT energy with zero-point energy and entropy via:

$$\Delta G = \Delta E + \Delta ZPE - T\Delta S,$$

where E is the DFT total energy, ZPE is the zero-point energy, T is the environmental temperature, and S is the entropy. For zero-point energy correction and entropy calculations, the vibrational frequencies were calculated by employing density functional perturbation theory. Considering the effect of solvation, we corrected the adsorption energy by using VASP

1.5 Photocatalytic activity test

H_2O/TEOA mixed solution containing EY photosensitizer and as-prepared cocatalysts was added into a gas-closed quartz reactor. Then, the quartz reactor was purged with Ar gas for 30 min. A 300 W Xe lamp (PLS-SXE300D, Perfectlight) with UV cutoff filter ($\lambda \geq 420$ nm) was applied to as the light source and the light intensity was measured to be 405 $mW.cm^{-2}$. The reactor temperature was hold at room temperature by an electronic fan. For each 2 h, the gaseous products were analyzed by gas chromatography (GC 7900, Techcomp). H_2 was analyzed by a thermal conductivity detector (TCD). Product gases were calibrated with the standard gas (H_2) **Fig. S10**. The recycling test of catalytic H_2 evolution over the as-prepared photocatalyst was done as follows. Typically, after the reaction of the first run under visible light irradiation, the photocatalyst was separated by filtration and washed with deionized water three times. Then, the fresh reaction solution containing EY-dye was mixed with the used cocatalysts to subject it to the second run photocatalytic activity test. The subsequent three runs of photocatalytic recycling tests were performed in a similar manner. The apparent quantum efficiency (AQE) of H_2 evolution was conducted under the same photocatalytic conditions. The apparent quantum efficiency (AQE) was calculated according to the equation below:

$$\mathrm{AQE} = \frac{\text{Number of reacted electrons}}{\text{Number of incident photons}} \times 100\%$$

$$= \frac{\text{Number of evolved } H_2 \text{ molecules} \times 2}{\text{Number of incident photons}} \times 100\%$$

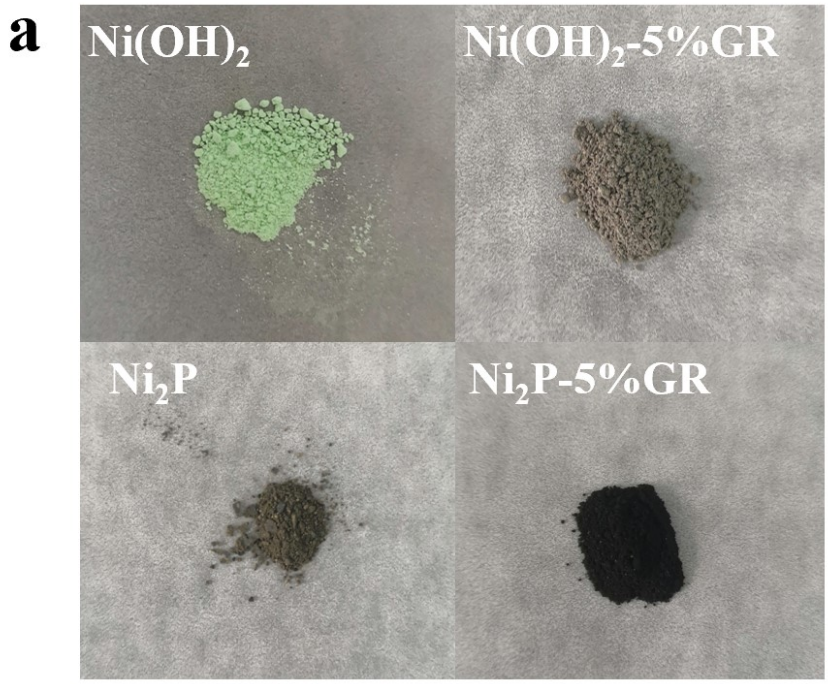

Fig. S1 Photographs of pristine $Ni(OH)_2$, Ni_2P, $Ni(OH)_2$-5%GR and the samples of Ni_2P-5%GR composites.

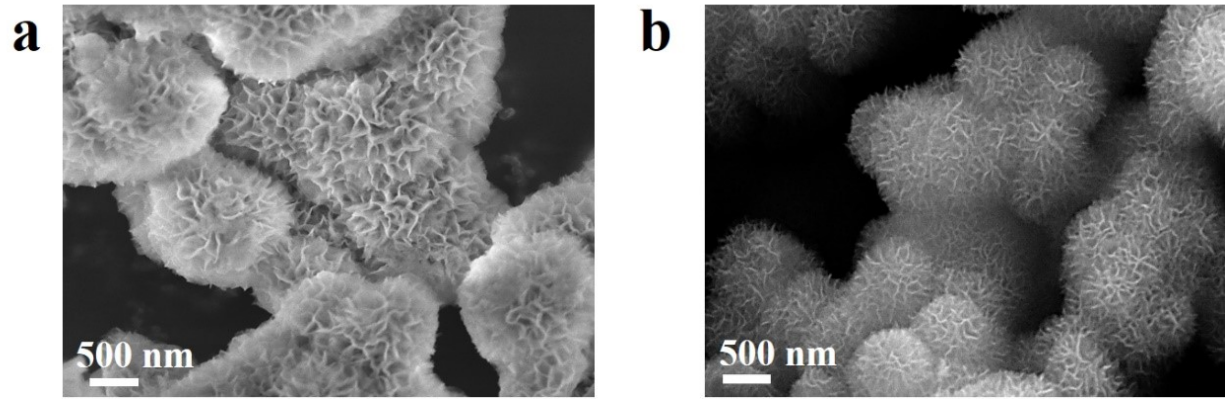

Fig. S2 SEM image of (a) $Ni(OH)_2$ and (b) Ni_2P.

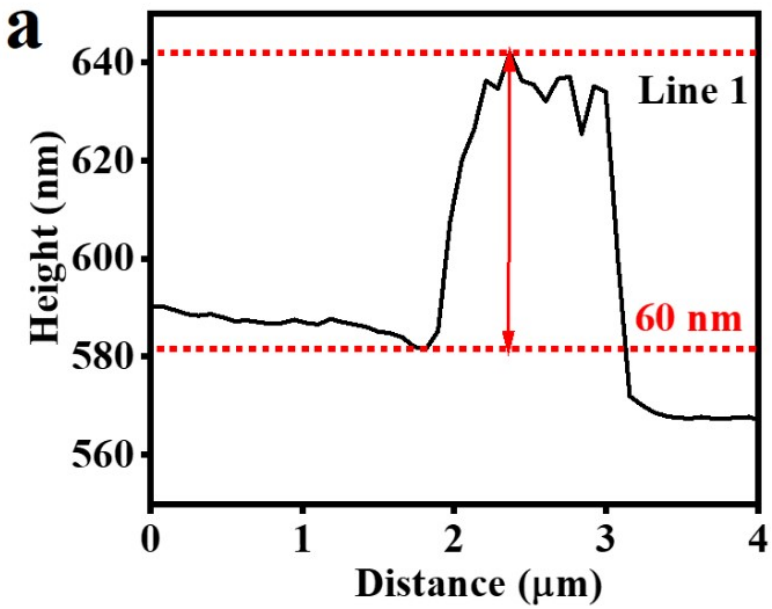

Fig. S3 Thickness information of Ni_2P-5%GR The corresponding height profiles along the (a) white line 1 drawn in **Fig. 1g**.

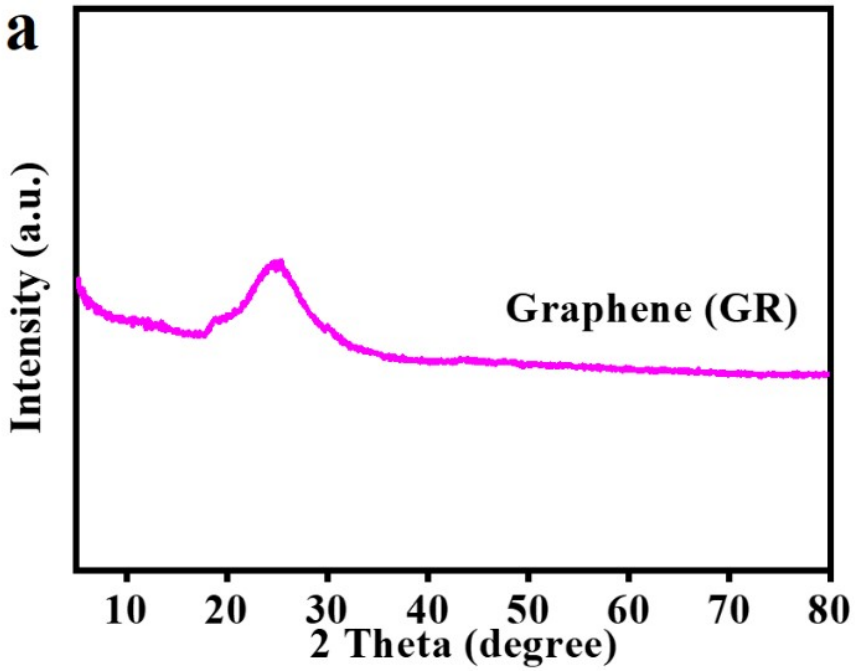

Fig. S4 XRD patterns of graphene (GR).

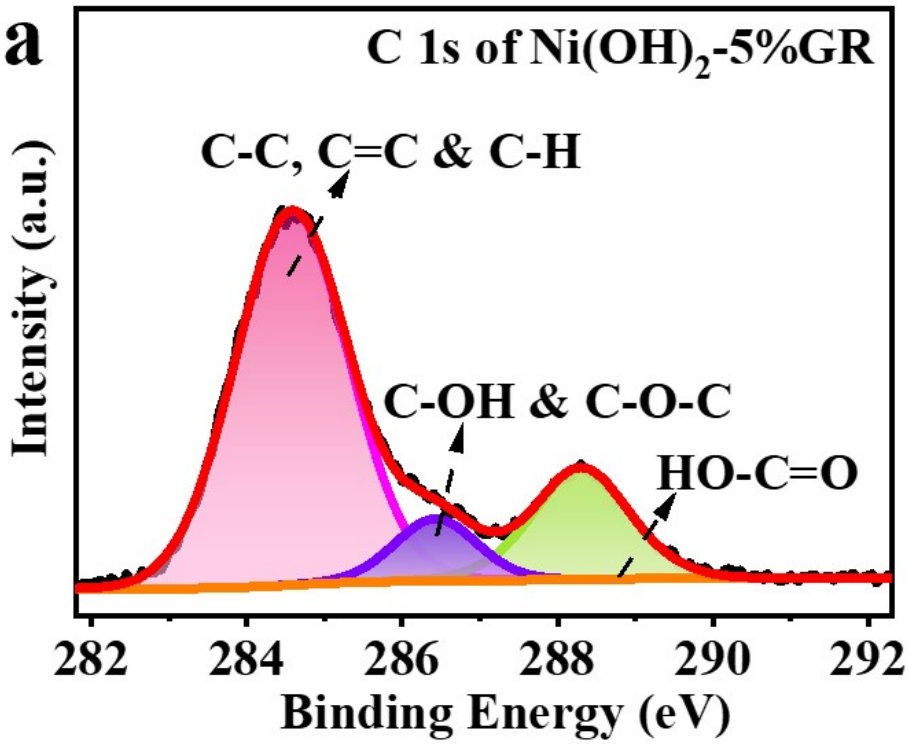

Fig. S5 High-resolution C 1s **XPS** spectrum of $Ni(OH)_2$-5%GR.

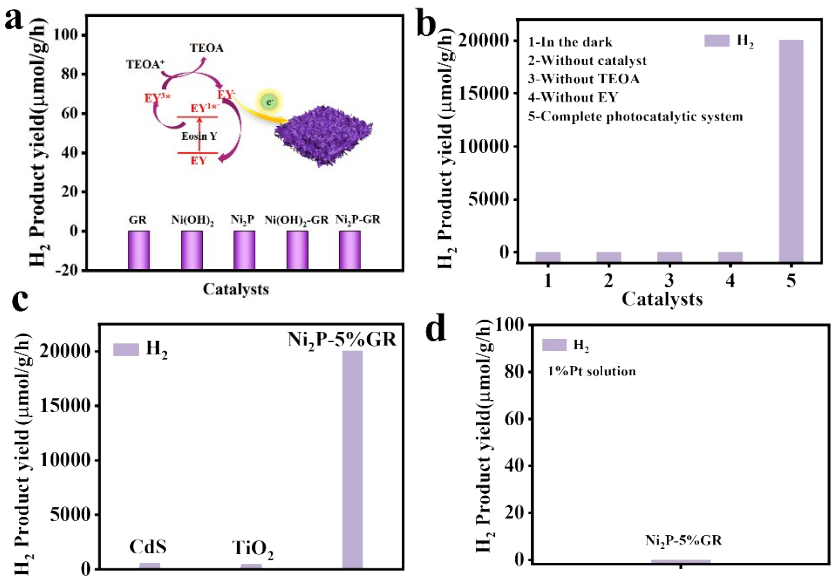

Fig. S6 (a)The control experiments for HER over the catalysts without the introduction of EY. (b) H_2 photoreduction properties of Ni_2P-5%GR under different experimental conditions. (c) Comparison of visible-light photocatalytic H_2 evolution activities between CdS, TiO_2 and Ni_2P-5%GR samples. (d) H_2 evolution activity of the optimized photocatalyst with 1%Pt solution without a sensitizer.

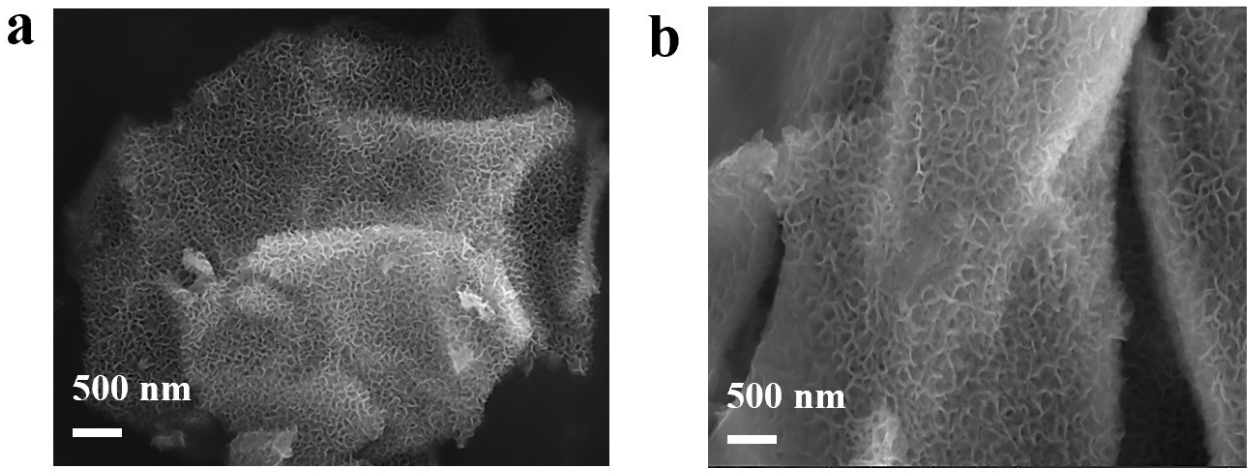

Fig. S7 SEM image of used Ni_2P-5%GR composite.

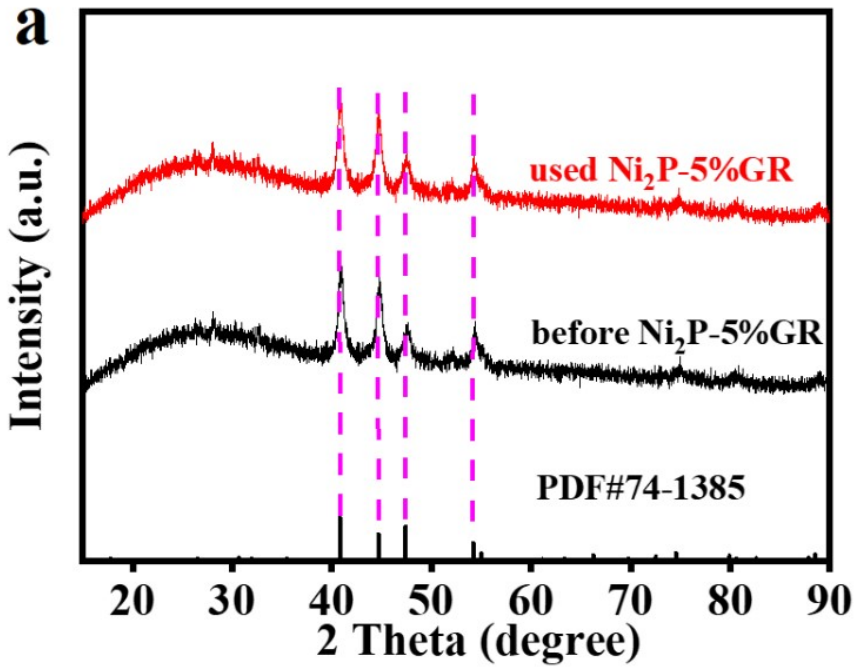

Fig. S8 XRD patterns of used Ni_2P-5%GR composite.

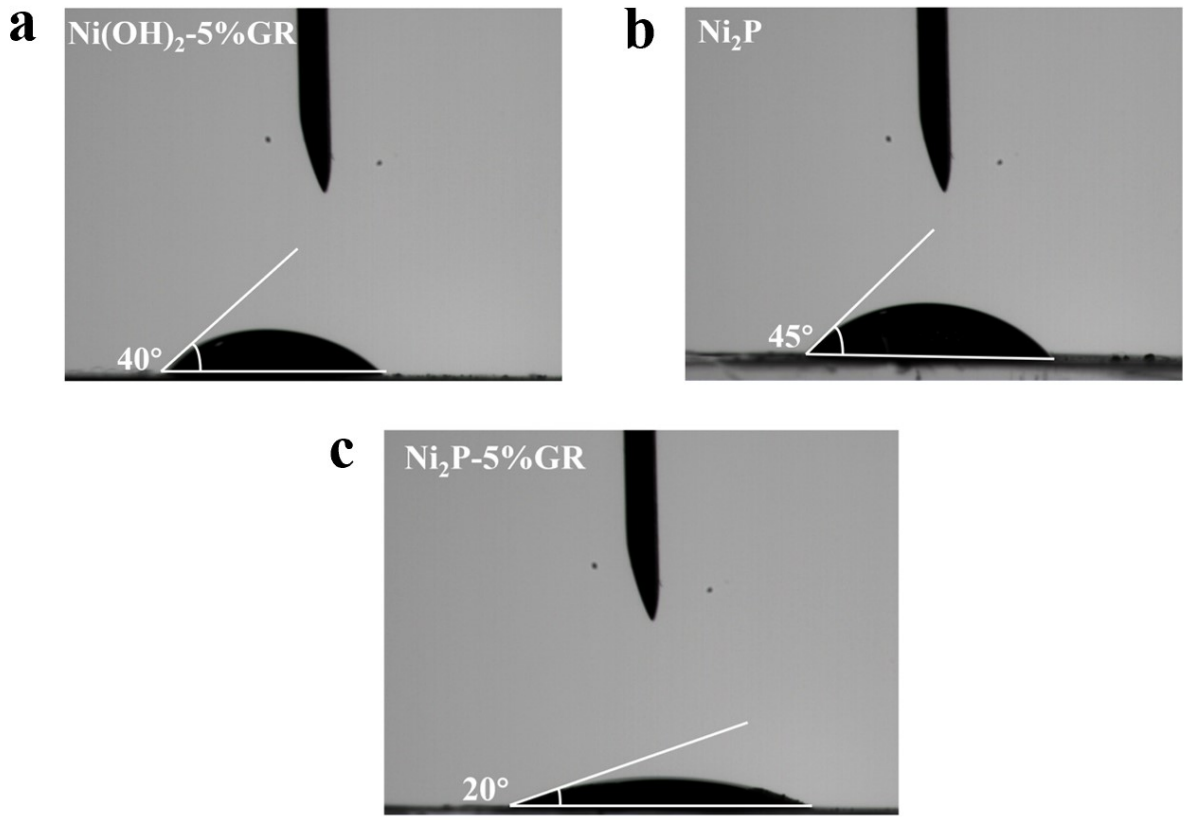

Fig. S9 Contact angle studies of (a) $Ni(OH)_2$-5%GR, (b) pure Ni_2P and (c) Ni_2P-5%GR composites.

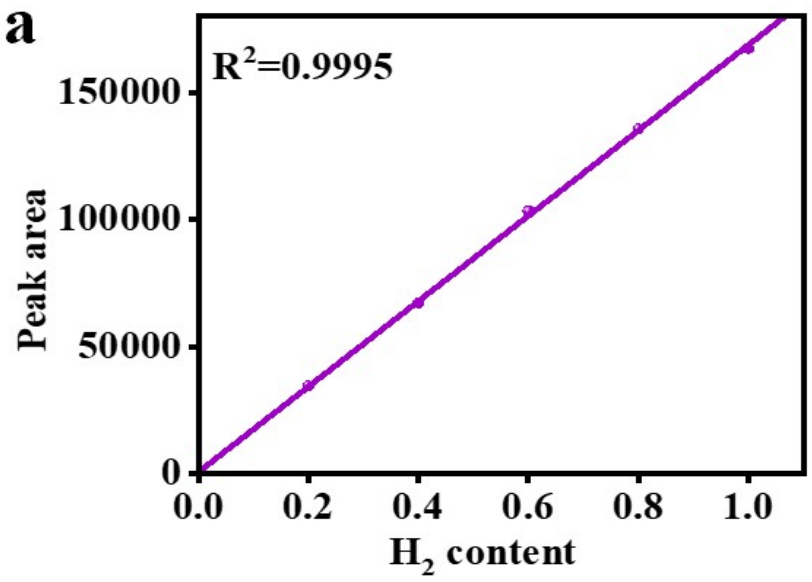

Fig. S10 Gas chromatography curves for H_2 standard under different contents.

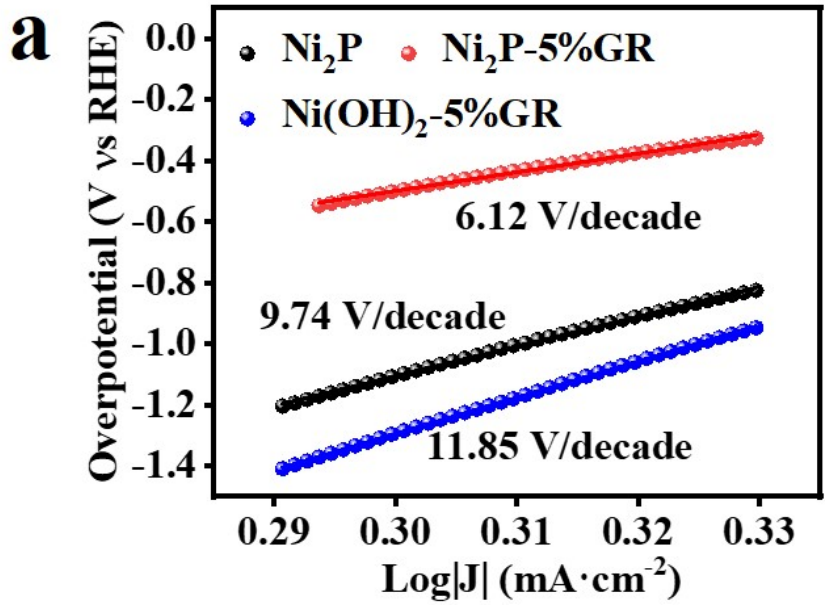

Fig. S11 Tafel slope diagrams of $Ni(OH)_2$-5%GR, Ni_2P and Ni_2P-5%GR composites.

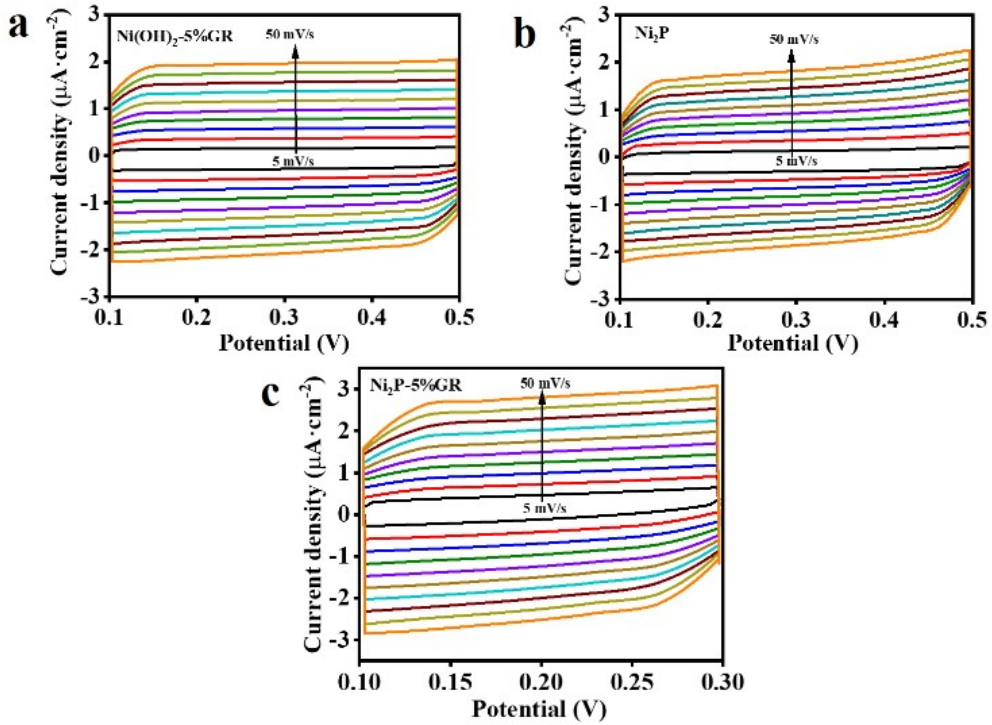

Fig. S12 The CV curves of (a) $Ni(OH)_2$-5%GR and (b) pure Ni_2P (c) Ni_2P-5%GR.

Note: Measurement of double layer capacitance (Cdl) for determining active electrochemical surface area (ECSA) of Ni_2P, $Ni(OH)_2$-5%GR and Ni_2P-5%GR CV curves with different scanning rate. Charging current density differences plotted against scanning rates. The linear slope (**Fig. 4e)** was used to present the ECSA.

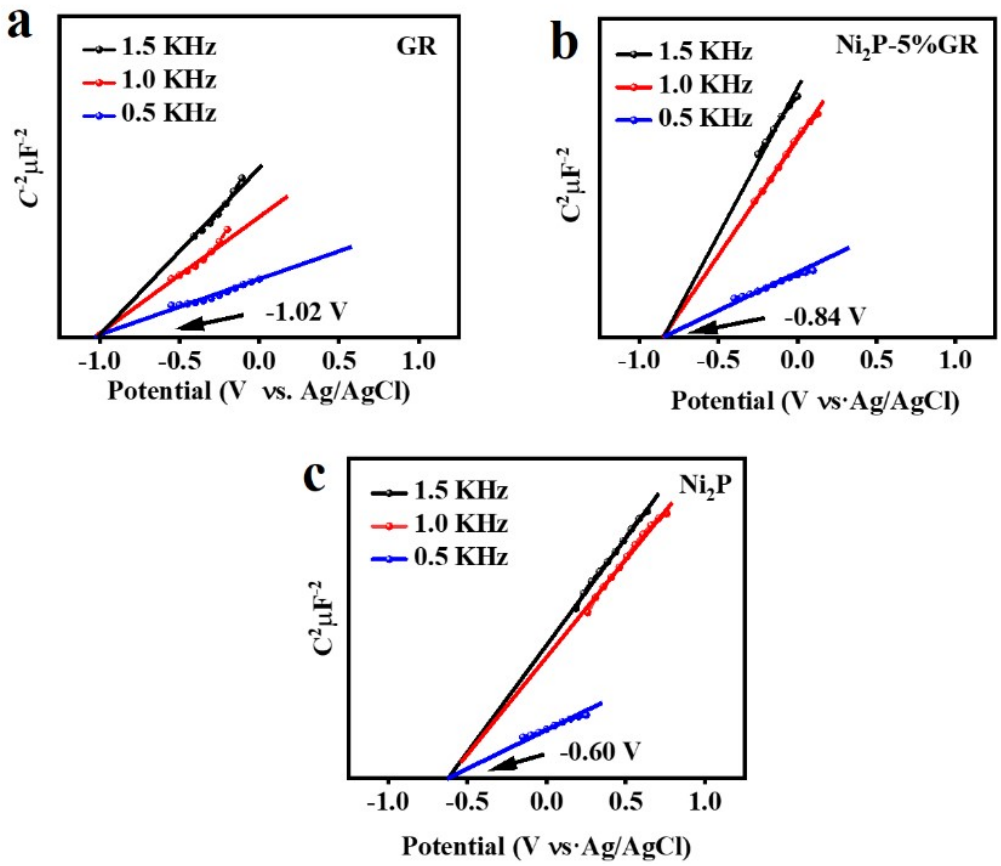

Fig. S13 Mott–Schottky plots of (a) GR and (b) Ni_2P-5%GR (c) bare Ni_2P

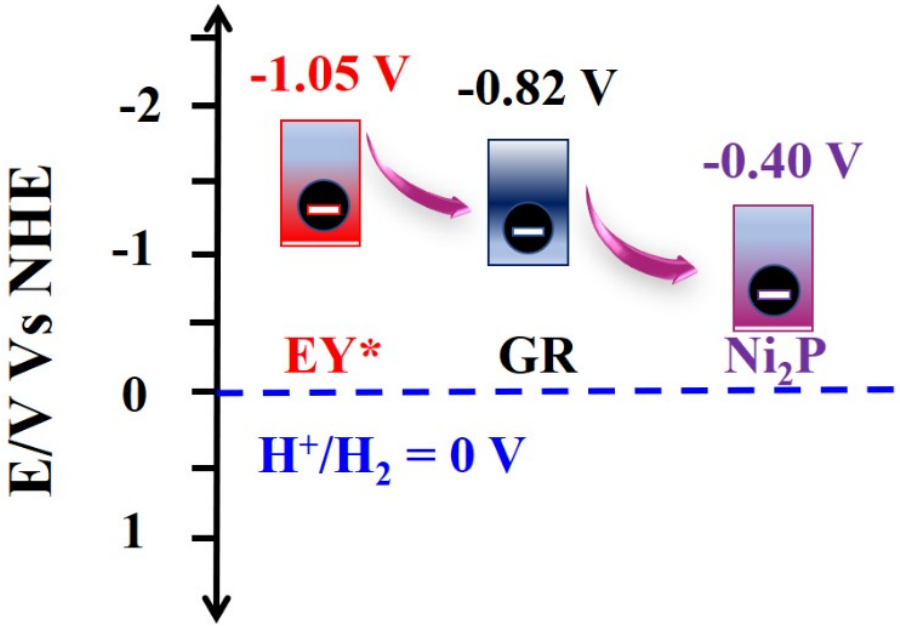

Fig. S14 Schematic energy-level diagram showing the electron transfer from EY* to GR and Ni_2P.

Table S1. Surface Areas of Samples.

Samples	BET surface area ($m^2 \cdot g^{-1}$)
$Ni(OH)_2$-5%GR	71.86
Ni_2P	39.87
Ni_2P-5%GR	140.51

Table S2 EIS equivalent circuit fitting results

Samples	Rs (KΩ)	Rct (KΩ)
GR	0.058	0.16
$Ni(OH)_2$-5%GR	0.083	0.63
Ni_2P	0.056	0.55
Ni_2P-5%GR	0.13	0.43

Table S3. Comparison of this work and other photocatalysts for photocatalytic hydrogen evolution.

Photocatalysts	photosensitizer	Light sources	Sacrificial agents	AQE (%)	Ref
Ni_2P-GR	EY	300 W Xe lamp; λ> 420 nm	TEOA	16.6	this work
UiO-66-NH_2	EY	300 W Xe lamp; λ> 380 nm	TEOA	11.6	1
MoS_2	EY	300 W Xe lamp; λ> 400 nm	TEOA	6	2
Ni–Bi/rGO	EY	300 W Xe lamp; λ> 420 nm	TEA	/	3
RGO/NiS_x	EY	300 W Xe lamp; λ> 420 nm	TEOA	12	4
NiO	EY	300 W Xe lamp; λ> 400 nm	TEOA	6.4	5
EY/$Co(bpy)_3^{2+}$/RGO	EY	300 W Xe lamp; λ> 420 nm	TEOA	7.4	6
g-C_3N_4/Pt/GO	EY	300 W Xe lamp; λ> 400 nm	TEOA	9.7	7
MOF-199/Ni	EY	300 W Xe lamp; λ> 420 nm	TEOA	12	8
$Co(OH)_2$-GR	EY	300 W Xe lamp; λ> 420 nm	TEOA	12.8	9

References

1 J. W. Shi, F. Chen, L. L. Hou, G. S. Li, Y. Q. Li, X. J. Guan, H. P. Liu and L. J. Guo, *Appl. Catal., B*, 2021, **280**, 119385.

2 S. S. Chou, N. Sai, P. Lu, E. N. Coker, S. Liu, K. Artyushkova, T. S. Luk, B. Kaehr and C. J. Brinker, *Nat. Commun.*, 2015, **6**, 8311.

3 M. Q. Yang, J. Dan, S. J. Pennycook, X. Lu, H. Zhu, Q. H. Xu, H. J. Fan and G. W. Ho, *Mater. Horiz.*, 2017, **4**, 885-894.

4 C. Kong, S. X. Min and G. X. Lu, *ACS Catal.*, 2014, **4**, 2763-2769.

5 C.-C. Shen, Y.-N. Liu, X. Wang, X.-X. Fang, Z.-W. Zhao, N. Jiang, L.-B. Ma, X. Zhou, T.-Y. Cheang and A.-W. Xu, *Dalton Trans.*, 2018, **47**, 11705-11712.

6 A. Lewandowska-Andralojc, A. Malolepszy, A. Stritt and A. Grohmann, *Catal. Sci. Technol.*, 2020, **10**, 4693-4702.

7 P. Wang, Z. Guan, Q. Li and J. Yang, *J. Mater. Sci.*, 2017, **53**, 774-786.

8 M. Zhang, X. Chen, X. Jiang, J. Wang, L. Xu, J. Qiu, W. Lu, D. Chen and Z. Li, *ACS Appl. Mater. Interfaces*, 2021, **13**, 14198-14206.

9 Y. Wei, J.-G. Hao, J.-L. Zhang, W.-Y. Huang, S.-b. Ouyang, K. Yang and K.-Q. Lu, *Dalton Trans.*, 2023, **52**, 13923-13929.